Chapter 4

Research and Supervision Results Obtained by Russian Scientists and Specialists during Implementation of Flight Scientific Programmes in cooperation and with assistance of Foreign Scientists and Specialists

CONTENT

4.1. Cosmic Rays Astrophysics

4.1.1. Partially ionized plasmas in astrophysics
(Skobeltsyn Institute of Nuclear Physics of Lomonosov Moscow State University)

Partially ionized plasmas are found across the Universe in many different astrophysical environments. They constitute an essential ingredient of the solar atmosphere, molecular clouds, planetary ionospheres and protoplanetary disks, among other environments, and display a richness of physical effects which are not present in fully ionized plasmas. This review provides an overview of the physics of partially ionized plasmas, including recent advances in different astrophysical areas in which partial ionization plays a fundamental role. We outline outstanding observational and theoretical questions and discuss possible directions for future progress.
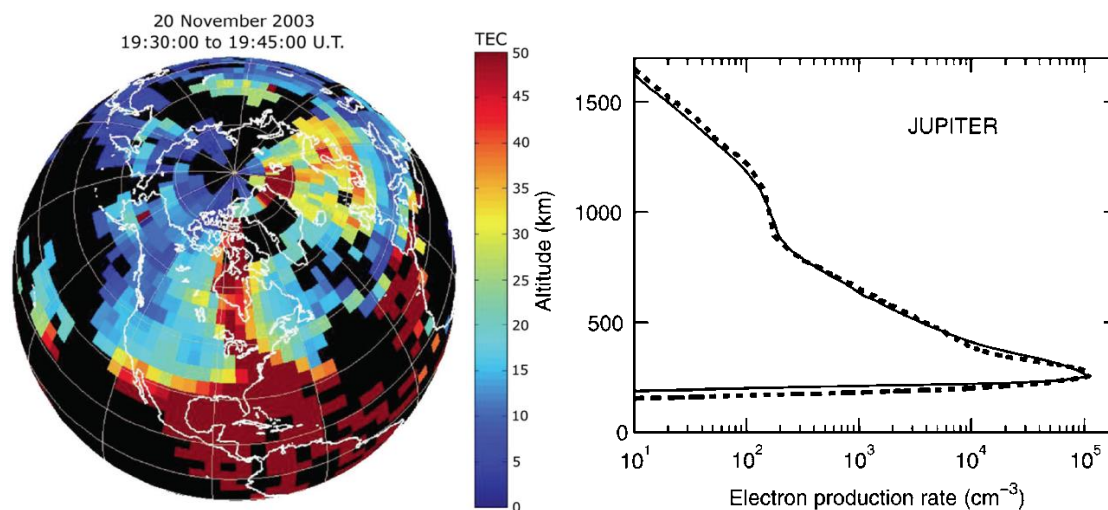

Fig.21. Storm-enhanced plasma density (SED) signatures in total electron content (TEC) observed on November 20, 2003. These are believed to be connected to plasmasphere erosion and driven by sub-auroral electric fields from the inner magnetosphere. Strong plasma density gradients are observed by a network of ground-based GPS observatories (figure courtesy of A. Coster).

Selected publication

Space Sci. Rev.

José Luis Ballester1 · Igor Alexeev2 · Manuel Collados3 · Turlough Downes4 · Robert F. Pfaff5 · Holly Gilbert6 · Maxim Khodachenko7 · Elena Khomenko3 · Ildar F. Shaikhislamov8 · Roberto Soler1 · Enrique Vázquez-Semadeni9 · Teimuraz Zaqarashvili7,10

4.2. X-Ray and Gamma-Astronomy

4.2.1. Observation of polarized hard X-ray emission from the Crab by the PoGOLite Pathfinder

(Skobeltsyn Institute of Nuclear Physics of Lomonosov Moscow State University)

We have measured the linear polarisation of hard X-ray emission from the Crab in a previously unexplored energy interval, 20–120 keV. The introduction of two new observational parameters, the polarisation fraction and angle stands to disentangle geometrical and physical effects, thereby providing information on the pulsar wind geometry and magnetic field environment. Measurements are conducted using the PoGOLite Pathfinder - a balloon-borne polarimeter. Polarization is determined by measuring the azimuthal Compton scattering angle of incident X-rays in an array of plastic scintillators housed in an anticoincidence well. The polarimetric response has been characterized prior to flight using both polarized and unpolarized calibration sources.We address possible systematic effects through observations of a background field. Themeasured polarization fractionfortheintegratedCrablightcurveis (18.4+9.8 −10.6)%, corresponding to an upper limit (99% credibility) of 42.4%, for a polarization angle of (142.2 ± 16.0).

Selected publications

«Observation of polarized hard X-ray emission from the Crab by the PoGOLite Pathfinder» Chauvin M., Floren H.-G., Jackson M., Kamae T., Kawano T., Kiss M., Kole M., Mikhalev V., Moretti E., Olofsson G., Rydstroem S., Takahashi H., Iyudin A., Fukazawa Y., Kataoka J., Kawai N., Mizuno T., Ryde F., Tajima H., Takahashi T., Pearce M., Monthly Notices of the Royal Astronomical Society: Letters, Volume 456, Issue 1, p.L84-L88, (02/2016) .
«The design and flight performance of the PoGOLite Pathfinder balloon-borne X-ray polarimeter».Chauvin M., Floren H.-G., Jackson M., Kamae T., Kawano T., Kiss M., Kole M., Mikhalev V., Moretti E., Olofsson G., Rydstroem S., Takahashi H., Lind J., Stroemberg J.-E., Welin O., Iyudin A., Shifrin D., Pearce M., Experimental Astronomy, Volume 41, Issue 1-2, pp. 17-41 (02/2016)

4.3. Space physics

4.3.1. The origin and early development stage of bipolar magnetic regions and sunspot groups
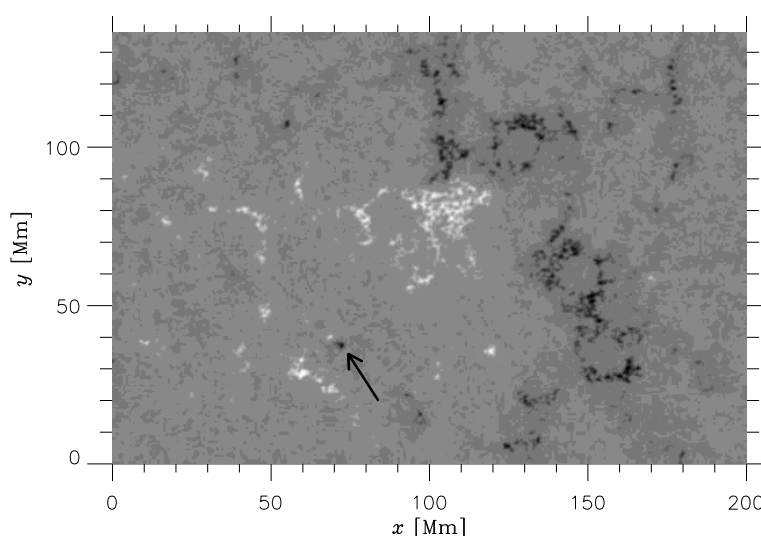
(Skobeltsyn Institute of Nuclear Physics of Lomonosov Moscow State University)

Procedures are developed for diverse processing of full-vector Hinode and SDO/HMI observational data for the magnetic and velocity fields in two conceived magnetic regions. This processing revealed some features of the field dynamics at the early evolutionary stage. The pattern of these processes proved to be in sharp contradiction with that following from the well-known model of the rising magnetic-flux tube.

Fig.30. A magnetogram illustrating the origin of a bipolar magnetic region. The arrow indicates a magnetic element of the leading polarity that has emerged in close neighbourhood to the trailing polarity.

Celected publications

A.V. Getling, R. Ishikawa, A.A. Buchnev, Doubts about the crucial role of the rising-tube mechanism in the formation of sunspot groups, Advances in Space Research, v. 55, no. 3, pp.

862–870, 2015, doi:10.1016/j.asr.2014.07.024.
A.V. Getling, R. Ishikawa, A.A. Buchnev, Development of active regions: flows, magnetic-field patterns and bordering effect, Solar Physics, v. 291, no. 2. pp. 371–382, 2016, DOI: 10.1007/s11207-015-0844-3.

4.3.2. GENERATION OF SUPERHEATED SOLAR WIND IONS ^{4}HE, O AND FE AT 1 A.U.

(Skobeltsyn Institute of Nuclear Physics of Lomonosov Moscow State University)

Investigated the energy spectra of ions of ^{4}He, O and Fe with energies 0.04–2 MeV/nucleon according to the ULEIS instrument on board space probe ACE during quiet time periods in 2006-2012 in the minimum of 23d cycle we have been allocated 35 of the periods during which ions in the solar wind streams from Equatorial Coronal Holes (ECH) were registered. The spectra of superheavy ions from ECH obtained here were approximated either by a power function or a combination of a power function and an exponential one. According to the Fisk and Gloeckler model, stochastic acceleration of ions in quiet time in a turbulent medium leads to the ion spectrum in the form of a product of power and

exponential functions, with the exponent $\gamma = 1.5$. In this study, the approximation of 98 spectra produced values of $2<\gamma<6$, which may indicate other conditions in the areas of particle acceleration in solar wind flows from ECH.
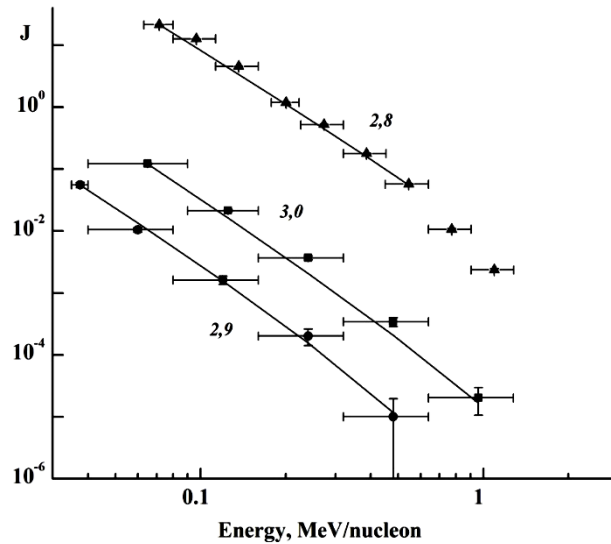

Fig.32. Energy spectra of 4He (triangles), O (squares), and Fe (dots) ions in the solar wind stream on August 6–9, 2009, at 1 AU from near-equatorial CH376. Solid lines show spectra approximations using the product of the power and exponential functions, J = (E–γ)exp(–E/E0).The values of the power indices γ for the ion spectra are given above the approximating lines. Ion intensity J is given in particles/(cm2 s sr MeV/nucleon).
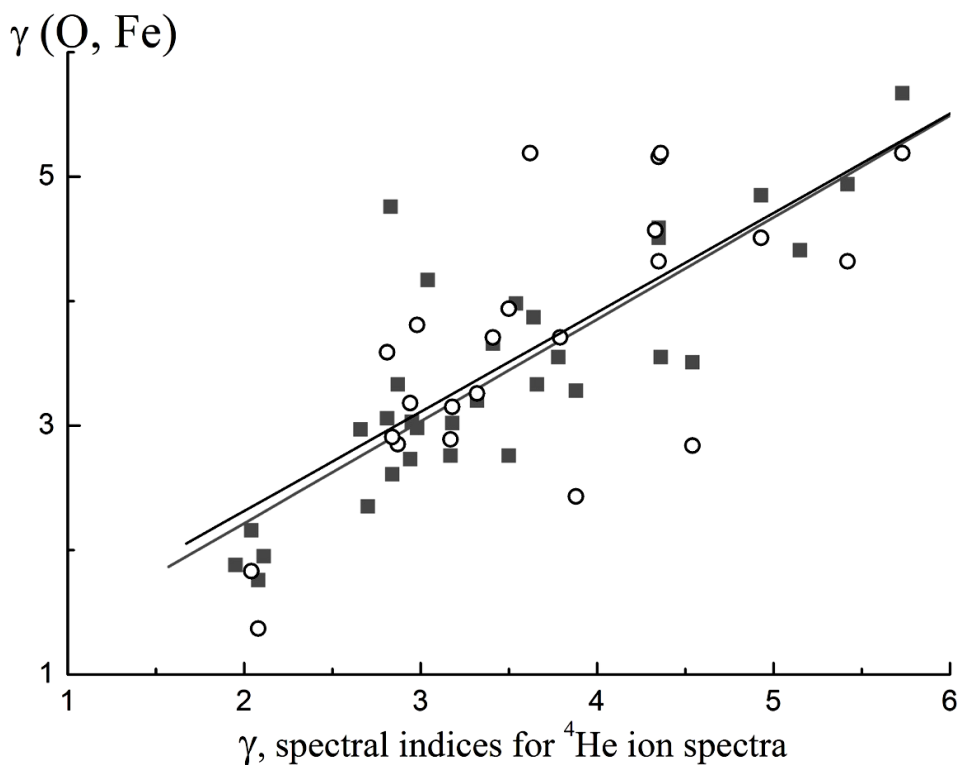
Fig.33. Energy spectra of superheated ions O (squares) and Fe (circles) depending on the parameters of the spectra of superheated ions 4E in the solar wind from 33 pre-Equatorial coronal holes in 2006-2010, the fluxes of superheated ions from these CD were determined and investigated according to ACE/ULEIS.

Selected publication
Zel'dovich, M.A., Logachev, Yu.I., Surova, G.M.,Kesckemety, K., and Veselovskii, I.S., Astron. Rep., 2016, vol. 60, p. 687.

4.3.3. The evolution of the charge state of the solar wind
(Skobeltsyn Institute of Nuclear Physics of Lomonosov Moscow State University)

Conducted a comprehensive study of multiple coronal mass ejections (CMEs) August 2-4, 2011, transient flows which caused strong geomagnetic disturbances of August 5, 2011. Kinematic and thermodynamic properties of expanding coronal structures using images from the space Observatory SDO/AIA in the EUV range and differential emission measure were studied for the observations of coronal sources and the formation of CME. Using the results of plasma diagnostics and MHD modeling, carbon ion (C6+/C5+) and oxygen ion (O7+/O6+) charge ratios were calculated, as well as the average charging state of iron ions Q<Fe> for CME as of August 2, 2011, taking into account the processes of heating, cooling, expansion, ionization and recombination of moving plasma in the corona to the "freezing" of the ion composition of solar wind plasma. The calculated values of the ion ratios and the average iron charge agree with the measured in-situ under the

assumption that the expanding plasma is heated by an additional source. The probable rate of plasma heating of CME in the low corona was estimated by comparing the calculated parameters of the ion composition of CME with the measured parameters in situ. The average heating power decreased from ~ 5-6 x 10^{-3} [erg cm⁻³s⁻¹] at 0.5÷1.5 solar radii to ~ 1–2 x 10-5 [erg cm⁻³s⁻¹] at 1.5÷5. Understanding the formation of transient flows in the solar corona is an important factor for modeling and forecasting space weather.

Selected publication

Rodkin D. D., Goryaev F., Pagano P., Gibb G., Slemzin V., Shugay Yu, Veselovsky I., Mackay D. H. Origin and Ion Charge State Evolution of Solar Wind Transitions during 4 – 7 August 2011Solar Physics, V 292, № 7, PPC. 90, 2017 DOI: 10.1007/s11207-017-1109-05.1.5.

4.3.4. Field-aligned currents observations close to Saturn

(Skobeltsyn Institute of Nuclear Physics of Lomonosov Moscow State University)

Field-aligned currents in the magnetosphere of Saturn have been reconstructed using CASSINImission data.
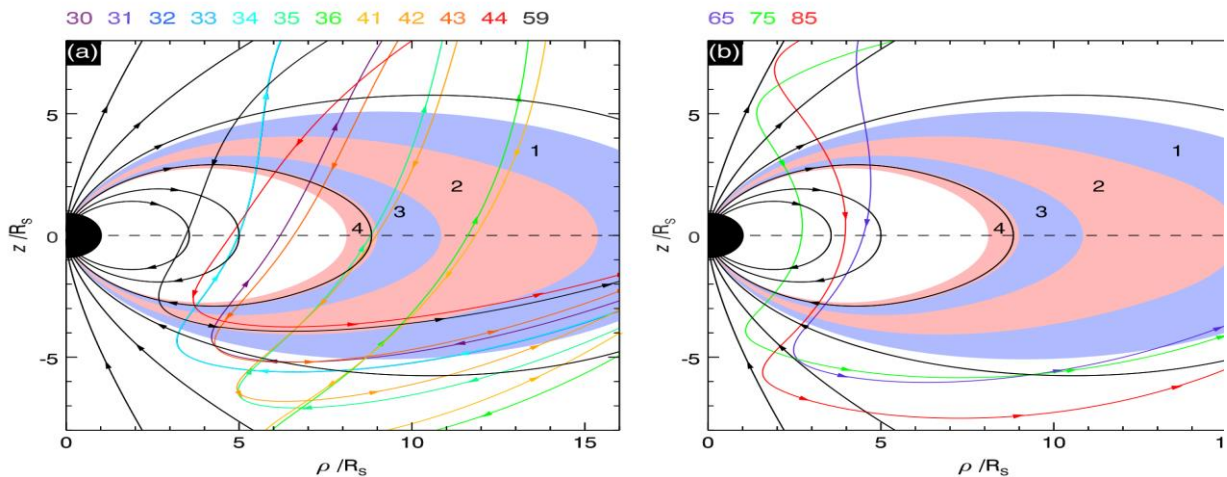

Fig. 47. CASSINI trajectories projected onto a magnetic meridian plane using cylindrical (ρ, z) coordinates, where z is distance along the planet's spin/magnetic axis positive northward and ρ is the perpendicular distance from the axis. (left) The trajectories of the 2006/2007 Revs employed in this study, Revs 30–36 and 41–44, plus Rev 59 from 2008, forming the dawn‑noon data set. (right) The trajectories are color‑coded as indicated at the top of each figure, and the arrows indicate the direction of travel. The black arrowed lines show model field lines starting at 5° intervals of southern colatitude between 0° and 30°. The colored bands, also bounded by field lines, show the averaged locations of the four independent field‑aligned current sheets determined from southern hemisphere data, numbered from pole to equator as shown, where the red and blue colors

represent the currents directed upward and downward relative to the southern ionosphere. The main auroral upward current corresponds to sheet 2.

4.4. Studies of Cosmic Gamma-ray Bursts from the Joint Russian-American KONUS-WIND Experiment on the U.S. Wind Spacecraft

(Russian Academy of Sciences, Ioffe Physical- Technical Institute,
NASA Goddard Space Flight Center)

Abstract

The joint Russian-American KONUS-WIND experiment on cosmic gamma-ray burst (GRB) studies has been successfully operating since November 1994 up to now onboard the U.S. Wind spacecraft with the KONUS Russian scientific instrument. Owing to its high sensitivity, exceedingly favorable location in the interplanetary space, and optimal observation program, the KONUS-WIND experiment is an unique source of information about the temporal and spectral characteristics of gamma-ray bursts through the 20 keV to 15 MeV energy range. These data constitute an essential element of the modern multi-wavelength studies of sources of gamma-ray bursts (GRBs) by spacecraft and by a network of terrestrial optical and radio telescopes.

1.   Experimental Approach

The joint Russian-American KONUS-WIND experiment consisting in study of cosmic gamma-ray burts has been operating onboard the U.S. Wind spacecraft since November 1994 up to now. The experiment employs the Konus scientific instrument created at the Ioffe Institute, Russian Academy of Sciences. The instrument operates in exceedingly favorable conditions for detection of gamma-ray bursts. The orbit of the spacecraft lies far outside the Earth's magnetosphere, which enables permanent all-sky observations and provides a stable radiation background, zero interference from the Earth's radiation belts, and no shadowing by the Earth.

The KONUS-WIND scientific instrument is a gamma-ray spectrometer having two identical gamma-ray detectors and an electronic unit for recording and preliminarily processing of the detector signals. Each detector comprises a NaI(Tl) spectrometric scintillation crystal 130 mm in diameter and 75 mm high, placed in a thin-walled aluminum container with a beryllium input window and an output window made of a highly transparent lead glass to protect the detectors from the soft background radiation. Such a detector provides a low (12 keV) threshold energy of radiation detection, up to 15 MeV detection range of gamma-ray photons with the energy resolution of 8.5 to 9.0% at the 660 keV Cs137 line, and event detection sensitivity on the order of 10^{-7} erg cm^{-2}. The detectors are allocated on

opposite faces of spacecraft stabilized by rotation, observing correspondingly the southern and northern celestial hemisphere in all-sky monitoring mode.

The instrument operates in two distinct modes: triggered burst detections and background measurements. It is self-triggering in that automatically records high temporal resolution burst data and energy spectra in on-board memory immediately, in response to a statistically significant increase in count rate. Burst time histories are recorded in three energy windows, G1 (20 - 70 keV), G2 (70 - 300 keV), and G3 (300 - 1100 keV), with a variable time resolution from 2 ms up to 256 ms. These records include prehistory sections of event time profiles recorded with 2 ms resolution. Up to 64 energy spectra are measured in the energy range 20 keV - 15 MeV. The accumulation time for each spectrum is automatically adapted to the current burst intensity within the range from 64 ms to 8 s.

The KONUS-WIND experiment has the following two advantages in comparison with other experiments now conducting GRB observations:

a) The instrument has a very convenient location for burst observations. The spacecraft spend almost all its time beyond the Earth magnetosphere, providing the key benefits of a constant radiation background, no occultation, and no interference originating in the Earth's radiation belts, resulting in extremely stable and practically uninterrupted observations.

b) The KONUS-WIND detector array constantly observes the whole sky omnidirectionally, with two instruments in symmetric, hemispherical modes, and thus is sensitive to essentially all GRBs that satisfy its trigger requirement, from the entire sky.

At present, the KONUS-WIND experiment is a unique source of most complete data regarding temporal, spectral, and energetic characteristics of cosmic gamma-ray bursts in the wide energy range from 20 keV to 15 MeV.

2.   Main results obtained during 2016-2017

2.1.   The second KONUS-WIND catalog of short gamma-ray bursts (GRBs) presents the results of a systematic study of 295 short GRBs detected from 1994 to 2010 (D.S. Svinkin at al, Astrophysical Journals. Supplement Series, 224:10, 2016). From the temporal and spectral analyses of the samples the catalog presents the burst durations, the spectral lags, the results of spectral fits with three model functions, the total energy fluences, and the peak energy fluxes of the bursts. An additional power-low spectral component and the presence of extended emission in a fraction of short GRBs are discussed. Two type of classification of short bursts connected with merger-origin and collapsar-origin are considered in tha catalog.
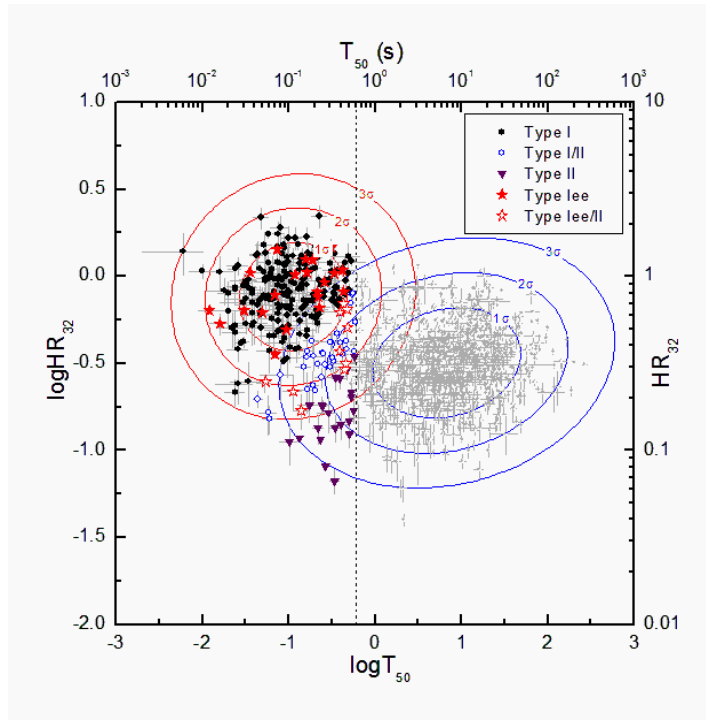
Fig. 1. Hardness-duration distribution of 1143 Konus-Wind bright GRBs. The distribution is fitted by a sum of two Gaussian distributions using the expectation and maximization (EM) algorithm. The contours denote 1σ, 2σ, and 3σ confidence regions for each Gaussian distribution. The vertical dashed line denotes the boundary ($T_{50}=0.6$ s) between long and short KW GRBs. The types for GRBs with $T_{50}<0.6$ s are shown in colors. Type I – merger origin, Type II – collapsar origin, Type I/II – uncertain type. Type Iee – short GRBs with extended emission (initial pulse was classified as Type I). Type Iee/II – short GRBs with extended emission (initial pulse was classified as Type I/II).
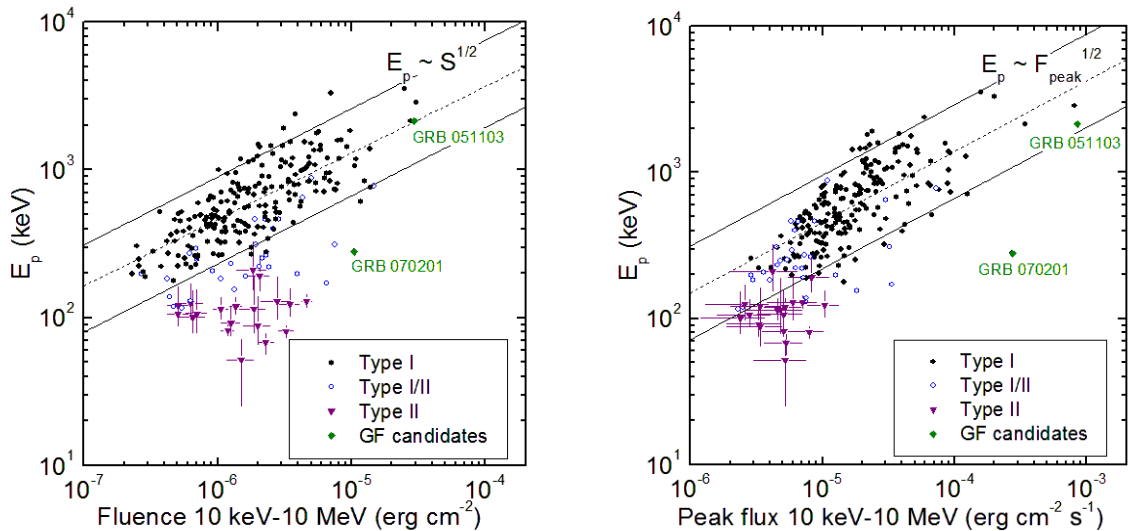

Fig. 2. Spectrum peak energy (E_p) as a function of the total energy fluence and the peak energy flux. Left panel shows E_p vs. the total energy fluence distribution for the Type I bursts (black circles); the bursts with uncertain type (empty circles); and the Type II bursts (triangles). Right panel shows E_p vs. the peak energy flux distribution for the same GRB groups. For the GRBs of type I and I/II error bars

are not shown. The extragalactic SGR giant flare candidates are shown with diamonds. The dashed lines denote the best powerlaw fits for the E_p–S and E_p–Fpeak (with an index of ~0.5) relations of the Type I GRBs. The solid lines denote the 90% prediction bands.

2.2. The KONUS-WIND Catalog of Gamma-Ray Bursts with Known Redshifts (A. Tsvetkova et al, Astrophysical Journal, 850, 161, 2017 December 1). The catalog presents the results of a systematic study of gamma-ray bursts (GRBs) with reliable redshift estimates detected in a triggered mode of the KONUS-WIND experiment during the period from 1997 February to 2016 June. The sample consists of 150 GRBs (including 12 short/hard bursts) and represents the largest set of cosmological GRBs studied to date over a broad energy band. From the temporal and spectral analyses of the sample, we provide the bursts durations, the spectral lags, the results of spectral fits with two model functions, the total energy fluences, and the peak energy fluxes. Based on the GRB redshifts, which span the range $0.1 \leq z \leq 5$ we estimate the rest frame, isotropic-equivalent energy, and peak luminosity. For 32 GRBs with reasonable constrained jet breaks, we provide the collimation-corrected value of the energetics. We consider the behavior of the rest-frame GRB parameters in the hardness-duration and hardness-intensity planes, and confirm the "Amati" and "Yonetoku" relations for Type II GRBs. The correction for the jet collimation does not improve parameter distributions and estimate the KONUS-WIND GRB detection horizon, which extends to z~16,6, stressing the GRB luminosity evolution, luminosity and isotropic-energy functions, and the evolution of the GRB formation rate, which are in general agreement with those obtained in previous studies.
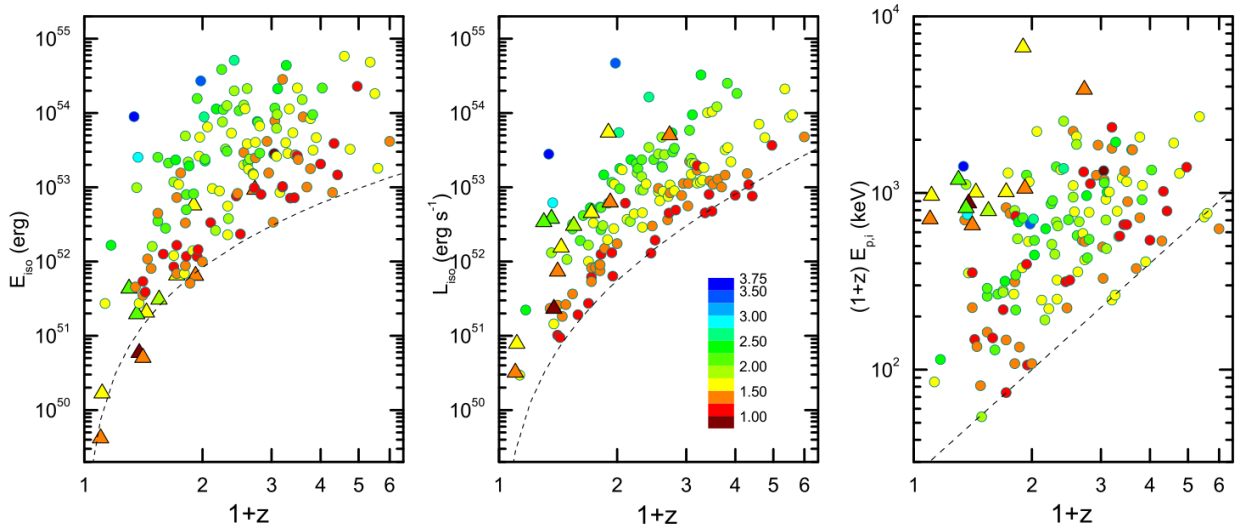

Fig. 3. Konus-Wind GRB isotropic equivalent gamma-ray energy (E_{iso}), isotropic-equivalent peak luminosity (L_{iso}), and rest frame peak energy ($E_{p,i,z}$) vs. redshift. The color of each data point (Type I: triangles, Type II: circles) represents the log of the burst's trigger significance in standard deviation of background counts. The observer-frame limits are shown with dashed lines.
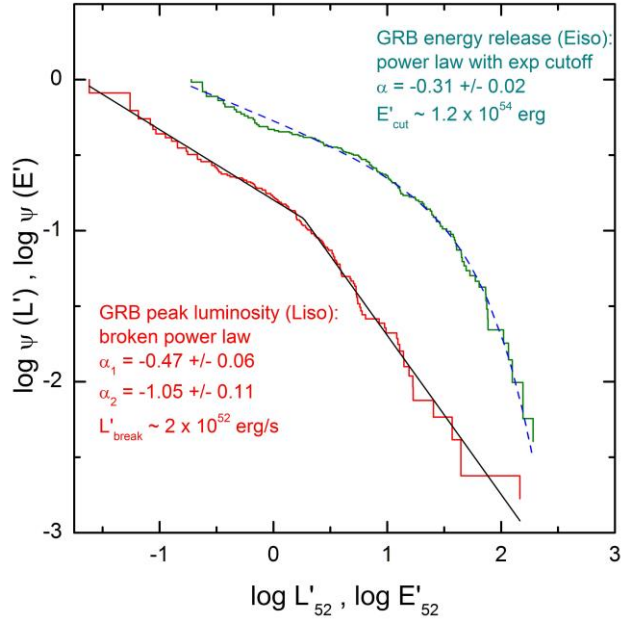
Fig. 4. Cumulative GRB isotropic-luminosity (LF) and isotropic-energy functions (EF). LF (red stepped graph) and EF (green stepped graph) estimated accounting for the luminosity and energy evolutions: $L' = L_{iso}/(1+z)^{1.7}$ и $E' = E_{iso}/(1+z)^{1.1}$. The distributions are normalized to unity at the dimmest points and a typical error bar is shown for each distribution. The solid and dashed lines show the best broken powerlaw and exponentially cutoff powerlaw fits for L' and E', respectively.
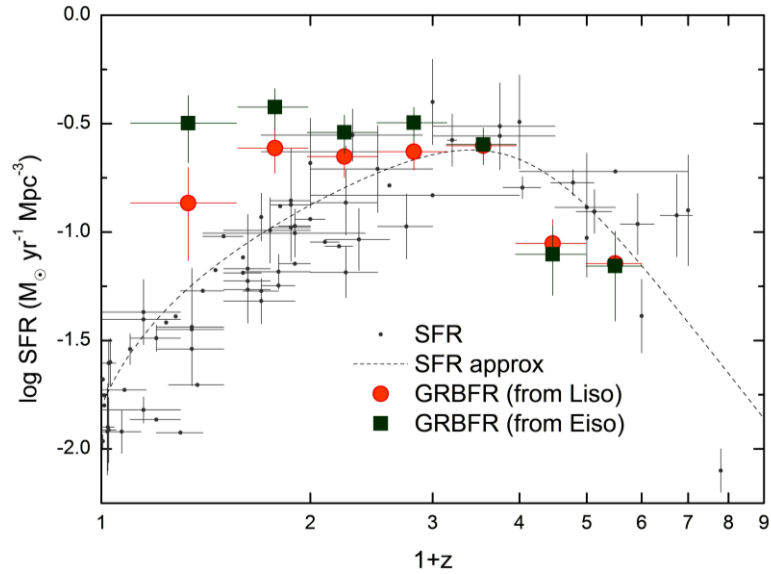

Fig. 5. Comparison of the derived GRB formation rate (GRBFR) and the star formation rate (SFR) data from the literature. The GRBFR was calculated using four data sets: z–L_{iso}' (filled circles) and z–E' (filled squares). The gray points show the SFR data from literature. The black solid line denotes the SFR

approximation from Li L.-X., MNRAS 2008, 388, 1487. The GRBFR points have been shifted arbitrarily to match the SFR at $(1 + z) \sim 3.5$.

2.3. One else investigation of GRBs with known redshifts was made according to KONUS-WIND an Fermi/GBM, two instruments that measure the spectral shape and the energetics of the prompt emission accurately (J.-I. Atteia…D.D. Frederiks et al., Astrophysical Journal, 837, 119, 2017 March 10). The GRBs are remarkable sources releasing huge amounts of energy on short timescales. Their prompt emission, which usually lasts a few seconds, is so bright that it is visible across the whole observational Universe. Studying these extreme events may provide clues on the nature of GRB progenitors and on the physical process at work in relativistic jets. We focus on GRBs within a range of redshifts z=1-5, a volume that contains a large number of energetic GRBs, and we propose a simple method to reconstruct the bright end of the GRB energy distribution from the observed one. We find that the GRB energy distribution cannot be described by a simple power law but requires a strong cutoff above 1-3 x 10^{54} erg. We attribute this feature to the intrinsic limit on the energy per unit of solid angle radiated by GRBs.

2.4. The KONUS-WIND data played an important role in the investigation of an extraordinary bright GRB 160625B, simultaneously observed in gamma-ray and optically wavelengths, whose prompt emission consists of three isolated episodes separated by long quiescent intervals, with the duration of each sub-burst being approximately 0.8 s, 35 s, and 212 s, respectively (B.B. Zhang,…R. Aptekar, et al, Nature Astronomy, vol. 2, January 2018, 69-75). Its high brightness allows us to conduct detailed time-resolved analyses in each episode, from precursor to main burst and to extended emission. The spectral properties of the first two sub-bursts are distinctly different, allowing us to observe the transition from thermal to non-thermal radiation between well-separated emission episode within a single GRB.

2.5. We have performed using KONUS-WIND instrument as basic segment of interplanetary network (IPN) a blind search for a gamma-ray transient of arbitrary duration and energy spectrum around the time of the LIGO gravitational-wave event GW150914 (K. Hurley, D.S. Svinkin at al, Astrophysical Journal Letters, 812, L12, 2016 September 20). Four GRBs were detected between 30 hr prior to the event and 6.1 hr after it, but none could convincingly be associated with GW150914. No other transients were detected down to limiting 15-150 keV fluences of $5x10^{-8} – 5x10^{-7}$ erg cm^{-2}. The search strategies and temporal coverage of the IPN on the day of the event are discussed and compared the spatial coverage to the region where GW150914 originate. It is reported about the negative result of a targeted search for the Fermi-GBM event reported in the conjunction with GW150914.

2.6. KONUS-WIND Solar Flare Database.
Data for all solar flares registered by the Konus-Wind instrument in the

triggered mode are available on-line via http://www.ioffe.ru/LEA/kwsun/ .
The database contains energy spectra and detector response matrices in
FITS format as well as light curves in G1, G2 and G3 channels in ASCII
and IDL SAV formats for solar flares detected in the triggered mode.
Detailed data description and instructions are also available on the database
website http://www.ioffe.ru/LEA/kwsun/kw-info.html. New solar
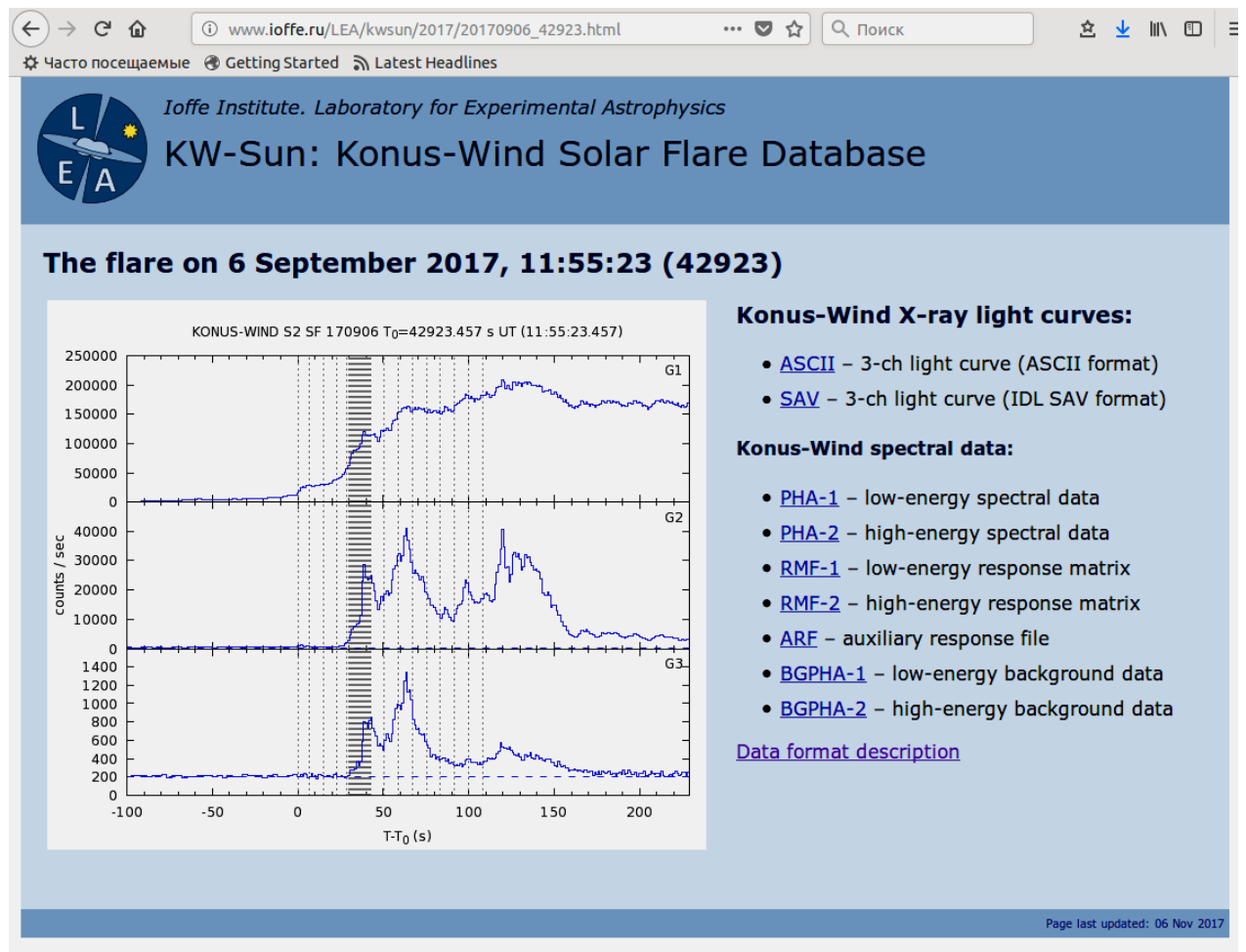observations will be added to the database as soon as they arrive.

Fig. 6. Webpage screenshot of the KONUS-WIND Solar Flare Database with
KONUS-WIND data on the X9.3 solar flare 2017-Sep-06.

KONUS-WIND energy range (now ~20 keV – 15 MeV) corresponds to the
emission of the electrons and ions accelerated in solar flares, and high temporal
resolution in the triggered mode allows to study fine structures of hard X-ray solar
emission. At the moment Konus-Wind is the only instrument in hard X-ray and
soft gamma-ray which observed two full solar cycles. KW-Sun solar flare
database is unique due to wide energy range, long observational period and the
absence of the Earth occultations.

Conclusions

The joint Russian-American KONUS-WIND experiment, which has already been operating for more than 23 years, provides important and frequently unique data regarding the various characteristics of GRBs and other types of transient gamma-ray emission in the 20 keV – 15 MeV energy range. Owing to the importance, quality, and completeness of the information obtained, the joint Russian-American Konus-Wind experiment has advanced to the forefront of the research into extreme explosive phenomena in the Universe.